Direct imaging of primary atomisation in the near-nozzle region of diesel sprays

V. Stetsyuk[1]*, C. Crua[1], R. Pearson[2], M. Gold[2]
[1]Centre for Automotive engineering, University of Brighton, UK
[2]BP Global Fuels Technology, Pangbourne, RG8 7QR, UK
*Corresponding author: v.stetsyuk@brighton.ac.uk

Abstract
In this publication we report on progress made with ongoing experimental investigations of the atomisation of n-dodecane using microscopic imaging and high-speed video with an ECN 'Spray A' injector. A long-distance microscope was used to visualize the near-nozzle region (1.025x0.906 mm). Our study focuses on the primary atomisation during the start, the steady-state and the end of the injection process. The spray formation and breakup of n-dodecane was investigated experimentally on a common rail diesel injector using a long working distance microscope. The objectives were to further the fundamental understanding of the processes involved in the initial stage of diesel spray formation under engine-like operating conditions, and provide validation data for numerical models. The end of injection was characterized by large ligaments and deformed droplets along with spherical droplets. It was noted that formation of large droplets during end of injection was not related to injection pressure. The large droplets were found to be in the range of up to 50 μm, which were moving with relatively low velocity. Typical velocity range for large droplets (30-50 μm) was between 1.5 to 5 m/s. The trajectory of individual droplets appeared to be random from injection to injection.

Introduction

Specific fuel consumption as well as pollutants of current and future diesel engines are directly related to combustion processes. It is expected that a number of vehicles, which use diesel engines will further grow in the future. Despite the fact that current diesel engines have lower specific fuel consumption and higher torque than gasoline engines, NO_x and soot emission may still be a problem [1]. Nitrogen oxide and soot emissions are strongly related to flame temperature and atomisation process [2-8]. The relationship between the combustion process and the spray parameters has been investigated, e.g. by [9-14]. It is quite obvious that fuel atomisation is among of top research priorities due to its direct relationship with pollutants formation.

A detailed characterisation of the near-nozzle region of diesel sprays is necessary in order to fully understand the physics of spray breakup. The modelling of the initial formation of ligaments (partially formed droplets) and subsequent breakup requires experimental data of good quality. At present, experimental characterisation of the initial stage of diesel spray formation is still inadequate, e.g. the distribution of droplets sizes, characterisation of individual droplets at the spray periphery, entire spray statistics etc. There is a number of publications discussing spray formation, liquid breakup processes, the effect of injection pressures on the microscopic spray characteristics [15-34].

Direct measurements of the droplet sizes under engine-like operating conditions are particularly challenging due to the harsh environment. The most traditional approach relies on high-speed video of an entire spray in order to characterise vapour and liquid penetration. The data, which is obtained during high-speed video measurements, cannot be used for detailed droplets sizing, especially when small droplets are considered. High resolution microscopic imaging seems to be a promising tool in understanding of droplets formation and breakup processes. It becomes an invaluable tool when analysing droplets motion and evaporation of single droplets.

However, there is a number of sources that contribute to the quality of the final post-processed image containing a range of liquid structures. These include motion blurring due to high jet and droplets velocities, optical aberrations and density gradients in an optical chamber. The density gradients in the optical chamber result in refractive index fluctuation, which in turn results in further image distortion.

Recently, the Engine Combustion Network (ECN) an international collaboration among experimental and computational researchers in engine combustion was initiated [35, 36]. The purpose of this collaboration is to provide experimental data, obtained under controlled and standardised operating conditions, as well as to provide a framework for collaborative comparisons of measured and modelled results. The ECN provides a framework for the

generation of rigorous experimental data of diesel spray experiments at engine conditions, which can be used for computational spray model development and comparison [35].

In this publication we report on work in progress that aims to characterise the atomisation of n-dodecane by microscopic imaging and high-speed video for an ECN Spray A injector. The target operating conditions were 22.8 kg/m^3, obtained with an in-cylinder pressure of 4.8 MPa and temperature of approximately 700 K). A long working distance dual-frame microscope was used to observe the near-nozzle region and track the periphery of the dense spray. Our study focuses on the primary atomisation during the start, the steady-state and the end of the injection process.

The remaining paper is structured as follows. The next section describes a reciprocating rapid compression machine (RCM), and the optical instrumentation used to study the injection process. The last section describes the results and discusses the findings. The paper ends with a summary of the main conclusions.

Material and methods

A reciprocating rapid compression machine (RCM), based on a Ricardo Proteus research engine, was used in this work. The RCM was a single-cylinder, two-stroke engine 135x150 mm with a displacement of 2.2 litres. The high pressure fuel pump was an electrically-driven pump connected to a common rail system and capable of delivering a rail pressure of up to 200 MPa. The injector (IFPEN 201.02 ECN Spray A) was a single hole bosh solenoid-actuated, generation 2.4, mini-sac, with 0.090 mm nominal nozzle outlet diameter. The nominal injection pressures were 50, 100 and 150 MPa. The injection pressure was carefully monitored and the difference between the target and the actual injection pressure was less than 0.2 MPa.

The illumination sources consisted of a pulsed high-speed monochromatic and incoherent diode laser operating at 690 nm for both the high-speed video and the microscopic imaging. A Phantom V710 high-speed camera was used to characterise the spray vapour penetration and a PCO Sensicam CCD camera was used for the microscopy. The high-speed camera was equipped with 80-200 mm Nikon AF Nikkor lens, which was used at its maximum aperture and zoom. The high-speed videos were recorded at 320 and 400 kfps with a field of view of 7 mm from the nozzle orifice. The nominal spatial scale factors were 32 µm/pixel for high speed video and 0.989 µm/pixel for the long-distance microscopy**.** In-cylinder pressure and temperature were 4.8 MPa and 700 K (corresponding to a density of 22.8 kg/m^3). The injection trigger pulse duration was 1.5 ms for all conditions.

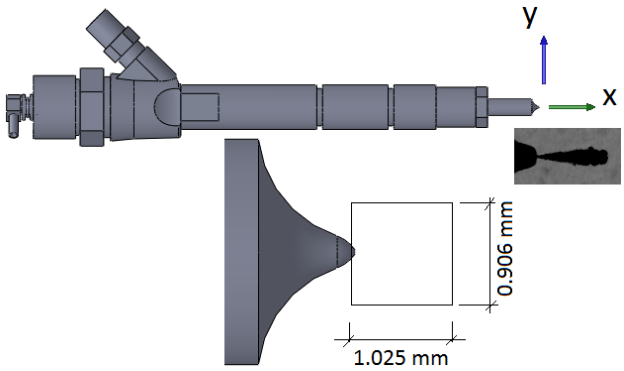

Figure 1: ECN Spray A injector coordinate system used in this work and control volume for microscopic imaging.

Table 1: Specifications for the injector used in this work

Description	Value	Units
Type	Bosh solenoid-actuated, generation 2.4	
Nominal nozzle outlet diameter	0.090	mm
Nozzle K factor*	1.5	
Nozzle shaping	Hydro-erosion	
Mini-sac volume	0.2	mm^3
Number of holes	1 (single hole)	
Orifice orientation	Axial (0^0 full included angle)	

* $K = \frac{d_{inlet} - d_{outlet}}{10}$

Table 2: Operating conditions and setup specification

Parameter	Value	Units
In-cylinder pressure (ICP)	4.8	MPa
Injection pressure	50, 100, 150	MPa
Injection duration (based on trigger)	1.5	ms
Fuel	n-dodecane	-
High-speed video scale factor	32	µm/pixel
Microscopy imaging scale factor	0.989	µm/pixel

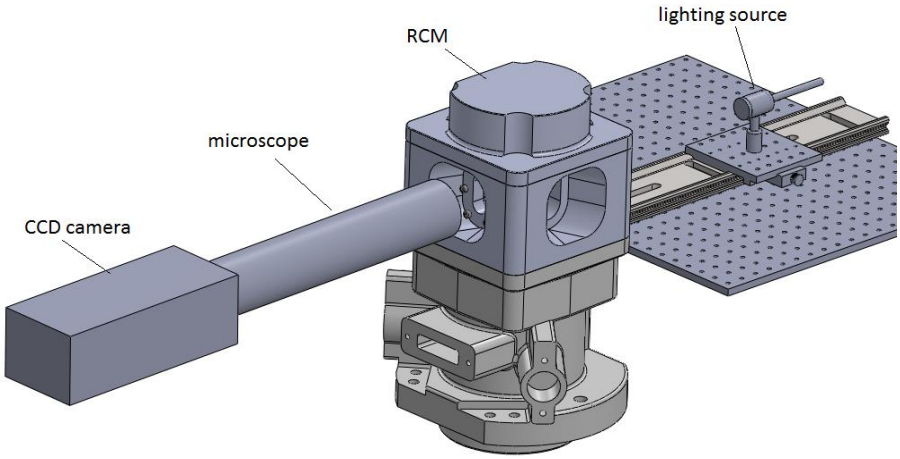

Figure 2: Experimental setup arrangement for microscopic imaging on the rapid compression machine (RCM). A pulsed high-speed monochromatic and incoherent laser diode with λ=690 nm was used as a lighting source.

Results and discussion

Figure 3 shows raw frames from a high-speed shadowgraphy video for several time steps after start of injection (ASOI), as well as a comparison of penetration measurements during motored conditions for ICP of 4.5 MPa with liquid and vapour penetration data from IFPEN [37] for the same injector (201.02). We used a set of MATLAB© code for image processing in order to extract vapour jet penetration, which was published by Sandia [38] for the processing of ECN data. The jet vapour-boundary is detected and plotted against time ASOI. Present measurements show that the measured penetration length lies within ± 1 standard deviation of published IFPEN data. Only penetration length from a single injection even is shown in Figure 3.

Figure 4 shows the liquid-vapour mixture exiting the nozzle hole for 0.295 ms ASOI for ICP of 4.8 MPa and injection pressure of 150 MPa. The most distinctive feature shown in this image is the so-called vapour pre-jet, which issues from the injector orifice prior to liquid jet. The vapour pre-jet is a well-defined axisymmetric mushroom-like vapour jet issuing sub-sonically into hot, still, compressed air [30]. The extent of this vapour pre-jet is circa 180 µm and does not vary from injection-to-injection significantly.

The vapour pre-jet can be caused by one or more of the following: expansion of cavitation pockets after previous injection; ingestion of in-cylinder gases after previous injection; heating and evaporation of fuel trapped inside orifice between injections. Figure 4 also shows fuel jet penetrating through vapour, which emerged prior to liquid. It can be suggested that this vapour consists of heated and evaporated fuel trapped inside the orifice, which can be ignited by the hot air mixed with remaining burnt products in a cylinder. It is also noted that the vapour pre-jet has clearly visible vortical structures, which can be seen under higher resolution (0.6 µm/pixel) [30]. The fuel jet continuous to penetrate the vapour pre-jet, as results, the vapour pre-jet cannot maintain the shape of a mushroom-like structure. Droplets can be seen to form at the jet periphery almost the instant the jet exits the nozzle. We observed droplets with typical diameter between 2 and 4 µm at the periphery of the spray during start and steady-state phases of injection.

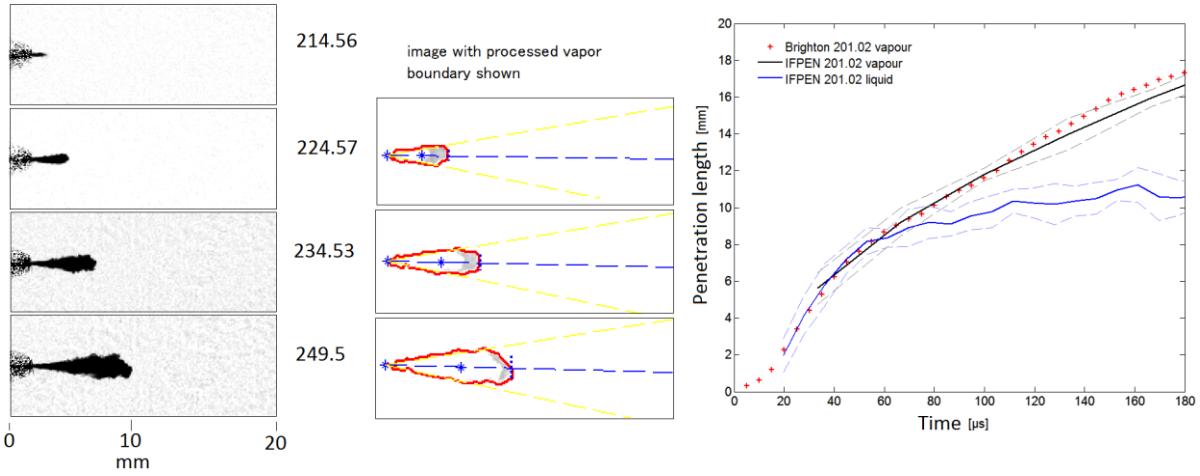

Figure 3: Frames for a high-speed shadowgraphy video as a function of time ASOI (μs). Example of processed images with spray boundary is also shown in red. On the right, penetration measurements during motored conditions for ICP of 4.5 MPa from a single injection compared with IFPEN data [37] and the same injector. The liquid and vapour penetration data is shown along with corresponding standard deviations (dashed lines).

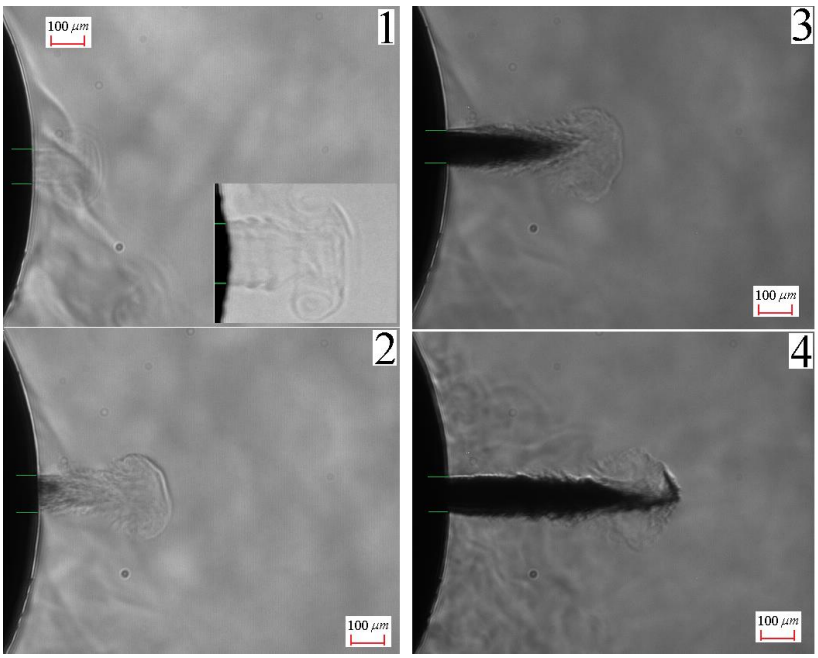

Figure 4: Liquid-vapour mixture exiting the nozzle hole for 0.295 ms after start of injection (ASOI) at injection pressure of 150 MPa. In-cylinder pressure (ICP) was 4.8 MPa. Vapour pre-jet is also shown under greater resolution as an insert on the top left image. The orifice is drawn as an overlay on the frames. Field of view is 1.025 x 0.906 mm.

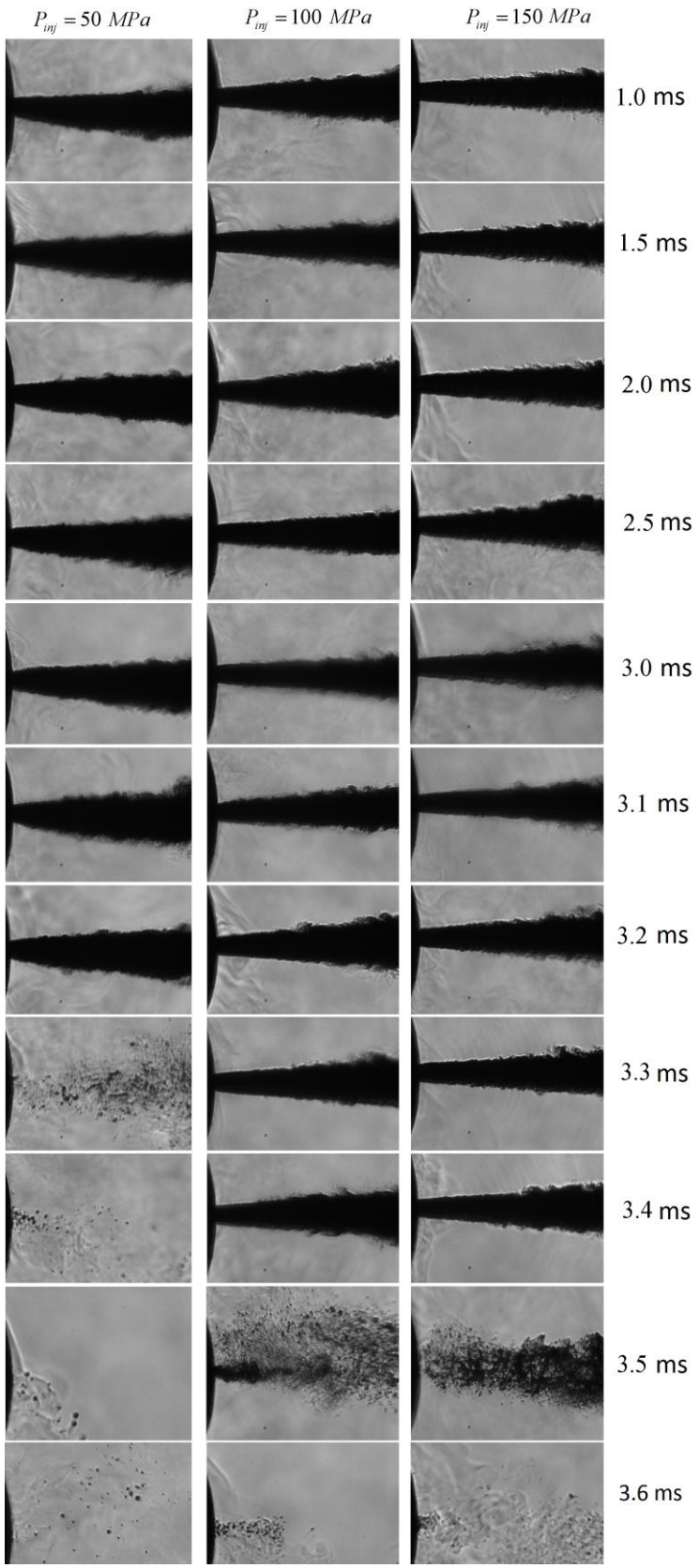

Figure 5: Steady-state and end of injection (EOI) for 50 (left), 100 (middle) and 150 (right) MPa as a function of time for 4.8 MPa gas pressure. All timings are after start of injection (ASOI) command. Each sequence represents field of view of 1.025 x 0.906.

Figure 5 shows an image sequence of spray evolution during steady-state period and the end of injection for different injection pressures. Note that the image sequence is built up from individual instantaneous realisations captured at different engine cycles. It should be emphasised that in order to build up an image sequence in such a way, a highly stable and reproducible injection event is essential. In this work it was observed through a series of instantaneous injection realisations that the spray was particularly stable and consistent during the steady-state.

Figure 5 clearly shows that for low injection pressure of 50 MPa the steady-state injection period is particularly long. The end of injection cannot be described to occur at a precise moment in time, but instead occurs over a non-negligible time span. The nominal trigger duration was 1.5 ms, however the injection process continues until 3.2 ms ASOI due to the small orifice diameter and the single-hole design. At 3.3 ms ASOI the spray becomes unstable and breaks down into a cluster of small and large droplets. It was also noted that large ligaments and highly deformed droplets were present. Large droplets emerging from the nozzle orifice were observed even at 3.6 ms ASOI. Intermediate and high pressures, i.e. 100 and 150 MPa demonstrate similar trend as low pressure spray. However, for these higher injection pressures a small secondary injection can be observed (for example at 3.5ms and 100 MPa in Figure 5). A third, and particularly small, injection event can be seen at 3.6 ms for 100 and 150 MPa.

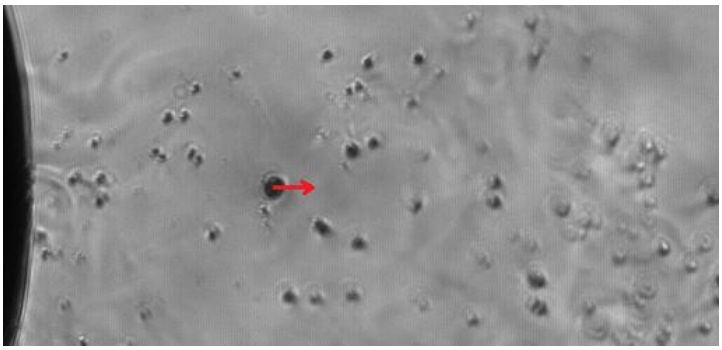

Figure 6: End of injection for injection pressure of 100 MPa and 3.7 ms ASOI. Droplet velocity vector is shown as red line (V_x=5, V_y=0 m/s). Field of view is 1.025 x 0.486 mm. Diameter of this droplet is 30 µm.

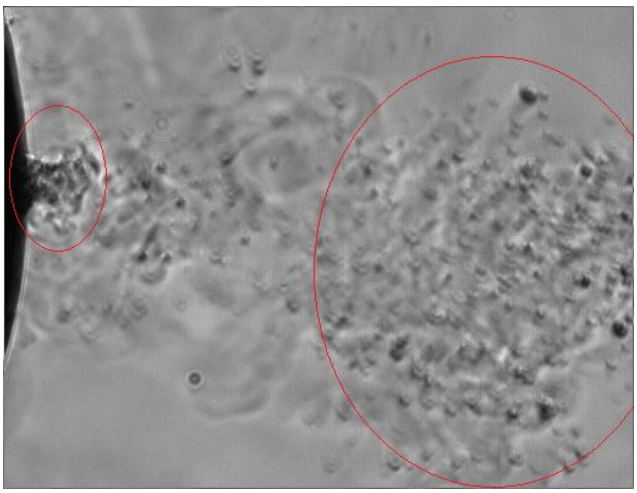

Figure 7: Micro injection events after the end of injection for injection pressure of 150 MPa for 3.6 ms ASOI. Field of view is 1.025 x 0.779 mm. A cloud of droplets from the end of injection is shown on the right as red encircled area.

The droplet shape during end of injection can often be approximated by a spheroid for high injection pressures i.e. 100 and 150 MPa. On the other hand, for low pressure sprays, i.e. 50 MPa, large ligaments as well as highly deformed droplets are observed (Figure 8). A detailed characterisation of the droplets shape, as well as their three-dimensional reconstruction, is needed in order to estimate the droplet surface area and volume, and ultimately better model their evaporation.

It has been observed that the trajectory of individual droplets during the end of injection can significantly vary from injection to injection. This can be related either to unsteady nature of the injection process at this stage or to the air motion during expansion stroke. Clearly visible vapour trails behind each droplet could be a sign of evaporation.

Figure 7 shows the end of injection for 3.6 ms ASOI and injection pressure of 150 MPa. Two zones are clearly visible, in which on the right hand side is a cloud of droplets formed after the end of injection. On the left hand side on the same Figure, a small cluster of droplets of various sizes is visible. These secondary micro-injection events could be caused by the needle bouncing from the seat, or from an expansion of the fluid in the sac.

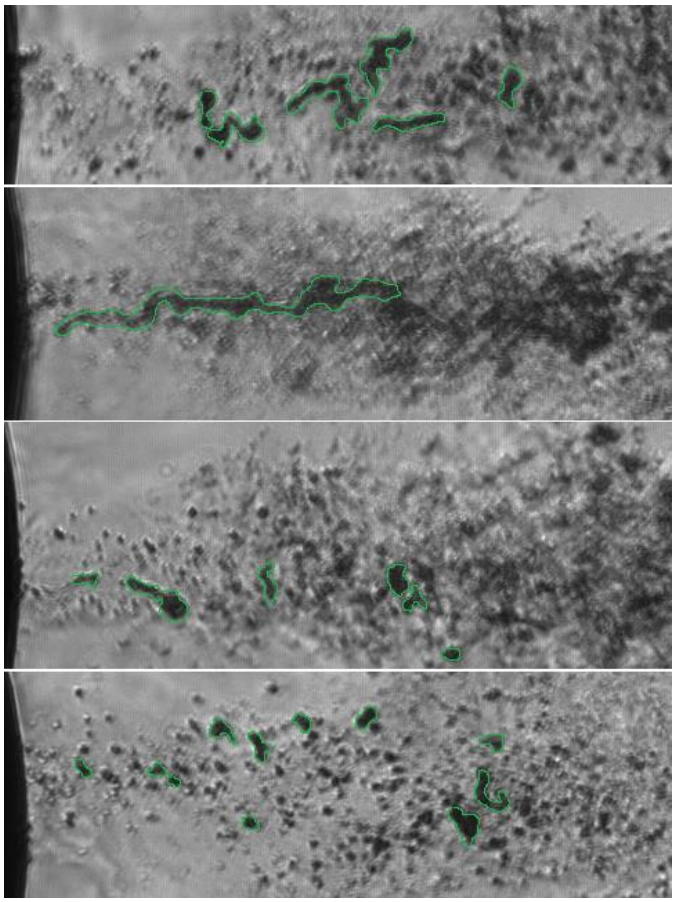

Figure 8: End of injection for injection pressure of 50 MPa and 3.3 ms ASOI. Ligaments and large deformed droplets with boundaries in green are also shown.

Conclusions

We presented ongoing experimental investigation of the atomisation of n-dodecane using long range microscopic imaging and ECN Spray A injector under engine-like operating conditions. Although it is particularly difficult to measure droplet sizes under such harsh operating conditions, especially at the fuel jet periphery and in the vicinity of the nozzle, long range microscopy can be a useful experimental method to investigate primary atomisation and breakup mechanisms.

The end of injection cannot be described to occur at a precise moment in time, but instead occurs over a non-negligible time span. The end of injection resulted in particularly large droplets compared to the main injection event. It was noted that formation of large droplets was not related to injection pressure. The large droplets were found to be in the range of up to 50 µm, which were moving with relatively low velocity. Typical velocity range for large droplet (30-50 µm) was between 1.5 to 5 m/s. The trajectory of individual droplets appeared to be random from injection to injection.

Acknowledgement
This work was supported by the UK's Engineering and Physical Science Research Council [grant number EP/K020528/1]. The authors are also grateful to BP International Ltd. for financial and technical support and to the EPSRC Engineering Instrument Pool for the loan of equipment used for this study.

References

[1] Heywood, J. B., 1988, "Internal combustion engine fundamentals."
[2] Lefebvre, A. H., 1982, "Gas Turbine Combustors".
[3] Lefebvre, A. H. 1995, Journal of Engineering for Gas Turbines and Power, 117, pp. 617–655
[4] Kouremenos, D. A. and Hountalas, D.T., 2001, SAE paper 2001-01-0198.
[5] Yang, F. and Minggao, O., 2003, SAE paper 2003-01-0351.
[6] Deepak, A., et al., 2011, Applied Energy, 88, pp. 2900–2907.
[7] Glassman, I., 1988, 22nd Symposium (International) on Combustion, 22, pp. 295–311.
[8] Pickett, L.M. and Siebers, D. L., 2002, Proceedings of the Combustion Institute, 29, pp. 655–662.
[9] Siebers, D. and Higgins, B., 2001, SAE Technical Paper 2001-01-0530.
[10] Higgins, D. and Siebers, D. L., SAE Paper No. 2001-01-0918, 2001.
[11] Yi, Y. and Reitz, R. D., SAE Paper No. 01-1041, 2003.
[12] Choi, C. Y. and Reitz R. D., 2000, Combust. Sci. Technol. 159, pp. 169–198.
[13] Arcoumanis, C. and Gavaises, M., 1998, Atomization Sprays 8, pp. 307–347.
[14] Patterson, M. A. and Reitz R. D., 1998, SAE Technical Paper 980131.
[15] Linne, M. A., et al., 2009, Proceedings of the Combustion Institute 32, pp. 2147–2161.
[16] Linne, M, et al., 2010, Experiments in Fluids, 49(4), pp. 911–923.
[17] Klein-Douwel, R.J.H., et al., 2007, Fuel, 86, pp. 1994–2007.
[18] Delacourta, E., et al., 2005, Fuel, 84, pp. 859–867.
[19] Mohammad, R. H., et al. 2013, Experimental Thermal and Fluid Science 50, pp. 10–20.
[20] Shoba, T. T. et al., 5-7 September 2011, 24th European Conference on Liquid Atomization and Spray Systems, Estoril, Portugal.
[21] Bae, C., et al., 2002, SAE 2002-01-1625.
[22] Badock, C., et al., 1999, International Journal of Heat and Fluid Flow, 20(5), pp. 538–544.
[23] Heimgärtner, C. and A. Leipertz, Pasadena, California, 2000, USA, July 16-20, 8th International Conference on Liquid Atomization and Spray Systems, .
[24] Shoba, T., et al., 5-7 September 2011, 24th European Conference on Liquid Atomization and Spray Systems, Estoril, Portugal,
[25] Sung, W. P, et al., 2006, International Journal of Multiphase Flow 32, pp. 807–822.
[26] Bae, C., et al., 2002, SAE Technical Paper 2002-01-1625.
[27] Heimgärtner, C. and Leipertz A., 2000, SAE 2000-01-1799.
[28] Lai, M.-C., et al., 1998, SAE 982542.
[29] Sjoberg, H., et al., 1996, Optical Engineering, 35(12), pp. 3591-3596.
[30] Crua, C., et al., 2010, SAE 2010-01-2247.
[31] Pickett, L.M., et al., 2011, SAE 2011-01-0686.
[32] Crua, C., et al., September 2-6 2012, 12th International Conference on Liquid Atomization and Spray Systems Heidelberg, Germany.
[33] Manin, J., et al., September 11-14 2012, THIESEL 2012 Conference on Thermo- and Fluid Dynamic Processes in Direct Injection Engines, Valencia, Spain.
[34] Pickett, L.M., et al., 2012, SAE 14PFL-1086.
[35] Engine Combustion Network website http://www.sandia.gov/ecn/ ([cit. 2014-06-22])
[36] Pickett, L.M., et al., 2010, SAE 2010-01-2
[37] Malbec, L., et al., 2013, SAE Int. J. Engines 6(3).
[38] www.sandia.gov/ecn/code.php ([cit. 2014-06-22])